Published in final edited form as:
Clin Cancer Res. 2011 April 15; 17(8): 2328–2338. doi:10.1158/1078-0432.CCR-10-2943.

Inhibition of prostate cancer osteoblastic progression with $VEGF_{121}$/rGel, a single agent targeting osteoblasts, osteoclasts, and tumor neovasculature

Khalid A. Mohamedali[1,*], **Zhi Gang Li**[2,†], **Michael W. Starbuck**[2], **Xinhai Wan**[2], **Jun Yang**[2], **Sehoon Kim**[1,§], **Wendy Zhang**[1], **Michael G. Rosenblum**[1,¥], and **Nora M. Navone**[2,¥]

[1] Department of Experimental Therapeutics, The University of Texas MD Anderson Cancer Center, Houston, TX 77030

[2] Department of Genitourinary Medical Oncology, The University of Texas MD Anderson Cancer Center, Houston, TX 77030

Abstract

Purpose—A hallmark of prostate cancer (PCa) progression is the development of osteoblastic bone metastases, which respond poorly to available therapies. We previously reported that $VEGF_{121}$/rGel targets osteoclast precursors and tumor neovasculature. Here we tested the hypothesis that targeting non-tumor cells expressing these receptors can inhibit tumor progression in a clinically relevant model of osteoblastic PCa.

Experimental Design—Cells from MDA PCa 118b, a PCa xenograft obtained from a bone metastasis in a patient with castrate-resistant PCa, were injected into the femurs of mice. Osteoblastic progression was monitored following systemic administration of $VEGF_{121}$/rGel.

Results—$VEGF_{121}$/rGel was cytotoxic *in vitro* to osteoblast precursor cells. This cytotoxicity was specific as $VEGF_{121}$/rGel internalization into osteoblasts was $VEGF_{121}$ receptor driven. Furthermore, $VEGF_{121}$/rGel significantly inhibited PCa-induced bone formation in a mouse calvaria culture assay. *In vivo*, $VEGF_{121}$/rGel significantly inhibited the osteoblastic progression of PCa cells in the femurs of nude mice. Microcomputed tomography analysis revealed that $VEGF_{121}$/rGel restored the bone volume fraction of tumor-bearing femurs to values similar to those of the contralateral (non–tumor bearing) femurs. $VEGF_{121}$/rGel significantly reduced the number of tumor-associated osteoclasts but did not change the numbers of peritumoral osteoblasts. Importantly, $VEGF_{121}$/rGel-treated mice had significantly less tumor burden than control mice. Our results thus indicate that $VEGF_{121}$/rGel inhibits osteoblastic tumor progression by targeting angiogenesis, osteoclastogenesis, and bone formation.

Conclusions—Targeting VEGFR-1 – or VEGFR-2–expressing cells is effective in controlling the osteoblastic progression of PCa in bone. These findings provide the basis for an effective multitargeted approach for metastatic PCa.

Keywords

metastasis; bone; prostate; osteoblast; osteoclast

[*]To whom correspondence should be addressed: 1515 Holcombe Blvd, Unit 44, Houston, TX 77030. Tel: 713-792-5954; Fax: 713-794-4261; kmohamed@mdanderson.org.
[†]Present address: Tianjin Medical University General Hospital & Tianjin Lung Cancer Institute, Tianjin, P.R. China
[§]Present address: GlycoFi/Merck & Co., Inc., Lebanon, NH
[¥]Joint senior authors

Potential conflicts of interest: The authors declare no conflicts of interest.

Introduction

Bone metastases are prevalent (90%) in patients with advanced prostate cancer (PCa) (1) and are a major cause of mortality and morbidity (2). Indeed, currently no curative therapy is available for men with PCa bone metastases, and only a modest survival advantage is achieved with chemotherapy. Skeletal metastases of PCa are unique in that they consistently produce bone-forming lesions, although an osteolytic component is also present (3–7). This high tropism for bone and the consistent osteoblastic phenotype suggests that PCa cells interact with bone and that this interaction influences the progression of the disease. Thus, bone-targeted therapies have been explored by many investigators as a new avenue for treating the disease.

We previously reported that $VEGF_{121}$/rGel, a vascular endothelial growth factor (VEGF) fusion construct composed of human $VEGF_{121}$ and the highly cytotoxic plant toxin gelonin (rGel), had efficacy against a model of prostate tumor growth in bone that had predominantly osteolytic features. We also found that $VEGF_{121}$/rGel targets mVEGFR-1^+ osteoclast precursor cells *in vitro* and reduces the number of mature osteoclasts at the tumor–bone interface *in vivo* (8). However, although osteoclast-targeted therapies are effective in controlling bone-related complications, clinical trials have failed to show a survival benefit in men with PCa bone metastases (9).

Numerous investigators have suggested that VEGF-A has a direct role in bone vascularization and formation during normal bone development (10–14), bone repair (12;13;15), and the bone-remodeling process that takes place in PCa skeletal metastasis (16;17). Indeed, the metastases of cancer cells to bone are known to alter bone architecture and mineral homeostasis, and tumor cells in the bone marrow generate a number of cytokines, including VEGF, that can directly affect the proliferation and maturation of osteoclasts, osteoblasts, and their precursors, markedly affecting bone remodeling (1;18;19). $VEGF_{121}$/rGel binds selectively to the VEGF receptors VEGFR-1 (Flt-1/FLT-1) and VEGFR-2 (Flk-1/KDR), which are normally overexpressed on the vasculature of most solid tumors (20–22), resulting in a reduction of angiogenesis (23–25). But again, clinical trials with antiangiogenic therapies failed to show a survival benefit in men with PCa bone metastases.

Thus, this work was undertaken to gain insight into the potential clinical relevance of the use of $VEGF_{121}$/rGel in men with PCa bone metastases. To that end, we evaluated the antitumor effect of $VEGF_{121}$/rGel in an osteoblastic model of castrate-resistant PCa growing in bone (MDA PCa 118 xenograft) (26). We also assessed whether $VEGF_{121}$/rGel had a direct effect on PCa-induced bone formation. Our findings suggest that osteoblast precursors are also a target of $VEGF_{121}$/rGel and that simultaneously targeting several cellular components of the bone microenvironment (including osteoblasts) will be an important therapeutic modality for controlling PCa growth in bone.

Materials and Methods

Cell Culture

Porcine aortic endothelial (PAE) cells transfected with the human VEGFR-2 receptor (PAE/KDR) and PAEs transfected with the human VEGFR-1 receptor (PAE/FLT-1) were a generous gift from Dr. Johannes Waltenberger (University Hospital, Maastricht, The Netherlands) and were propagated as previously described (27). The number of VEGFR-2 and VEGFR-1 receptor sites on these cells have been determined to be 150,000 and 50,000 per cell, respectively (28). Murine brain endothelial cells (bEnd.3) and human umbilical vein

endothelial cells (HUVECs) were kind gifts from Dr. Sophia Ran (Southern Illinois University, Springfield, IL). Human PCa cell lines PC-3, LNCaP and C4-2B, and the mouse preosteoblast cell line MC3T3-E1 were purchased from the American Type Culture Collection (Manassas, VA). Differentiation of confluent MC3T3 cells was performed as previously described (29) and confirmed by Alizarin Red S staining (30). Primary mouse osteoblasts (PMOs) were obtained from CD1 mice as reported previously (29). MDA PCa 2b (31) and MDA PCa 118b (26) cell lines are a bone-derived PCa cell line and xenograft, respectively, established in Dr. Nora Navone's laboratory. MDA PCa 118b cells were maintained *in vivo* by subcutaneous passage in immunodeficient mice (26).

Animals

Male athymic Balb/c nude mice (National Cancer Institute, Frederick, MD) were maintained under specific pathogen–free conditions according to the American Association for Accreditation of LaboratoryAnimal Care (AAALAC) standards.

Purification of $VEGF_{121}$/rGel

$VEGF_{121}$/rGel construction and purification were performed essentially as previously described (25), followed by SP Sepharose chromatography (pH 6.0) with a NaCl gradient to separate the biologically active dimeric form from other species. $VEGF_{121}$/rGel was concentrated and stored in sterile PBS at −20 °C.

Cytotoxicity and Internalization of $VEGF_{121}$/rGel and rGel

Cytotoxicity of $VEGF_{121}$/rGel, rGel, and $VEGF_{121}$ against log-phase MC3T3, PMO, MDA PCa 2b, and C4-2B cells was evaluated over 72 h as previously described (25). Cytotoxicity against 50,000 or 100,000 MDA PCa 118b cells was evaluated in short-term cultures obtained from subcutaneous tumors and grown over 72 h in CnT52 medium. Cytotoxicity against differentiated MC3T3 cells was evaluated after the cells were grown in differentiation conditions for 1, 2, or 3 weeks. For internalization, PMOs were treated with 4 μg/ml (48 nM) $VEGF_{121}$/rGel for 24 h and then washed with glycine buffer (500 mM NaCl, 0.1 M glycine, pH 2.5) to remove cell surface–bound $VEGF_{121}$/rGel. Cells were incubated with a rabbit anti-gelonin polyclonal antibody (1:200) followed by a FITC-conjugated anti-rabbit secondary antibody (1:80). Nuclei were stained with propidium iodide (1 μg/ml) in PBS. The cells were mounted on slides with 1,4-diazabicyclo[2.2.2]octane and visualized under a fluorescence microscope (Nikon Eclipse TS1000).

RNA Extraction

Total RNA was extracted using an RNeasy mini-kit (Qiagen, Valencia, CA), and its integrity was verified by electrophoresis on a denaturing formaldehyde-agarose gel and on a 2100 Bioanalyzer (Agilent, Foster City, CA).

Polymerase Chain Reaction (PCR) and Reverse Transcription (RT)-PCR Analysis

Relative levels of VEGFR-1, VEGFR-2, and VEGF-A transcript were assessed by RT-PCR analysis. GAPDH primers were used as controls (24). mVEGF transcript was detected using primers previously described (8). We utilized primers for VEGFR-1 and VEGFR-2 that recognize conserved sequences in both mouse and human cDNA (24), and also generated the following primers unique to mouse VEGFR: M R2 forward − 5′ TCTGTGGTTCTGCGTGGAGA; M R2 reverse − 5′ GTATCATTTCCAACCACCCT; M R1 forward − 5′ CTCTGATGGTGATCGTGG; M R1 reverse − 5′ CATGCCTCTGGCCACTTG. Amplified RT-PCR products were subjected to densitometric analysis using FluorChem8900 (Alpha Innotech, San Leandro, CA).

Organ Culture Bone-Formation Assay

Calvariae from 4-day-old CD1 mice (Charles River Laboratories International, Inc., Wilmington, MA) were excised, cut in half, and cultured for 7 d in six-well plates as previously described (26). Briefly, calvariae were placed on a metal grid bathed in BGJ medium (Sigma-Aldrich, St. Louis, MO) with 0.1% bovine serum albumin in the presence and absence of 100 nM $VEGF_{121}$/rGel or MDA PCa 2b cells cultured in the wells. The medium was changed on day 3, and $VEGF_{121}$/rGel was supplemented as appropriate. At the end of culturing, the calvariae halves were processed as previously described (26). Sections were also stained with hematoxylin and eosin (H&E). Histomorphometric analysis was performed by the Bone Histomorphometry Core facility at The University of Texas MD Anderson Cancer Center (M.W.S). Osteo II software version 8.40.20 (Bioquant, Nashville, TN) was used to measure the ratio of osteoid volume to bone volume, the ratio of osteoid surface to bone surface, and the osteoid area. Measurements of all samples were obtained approximately 160 μm from the frontal suture of the calvaria for a distance of 2 mm. The osteoid covering the bone was measured first, followed by the total bone surface; the degree of bone surface covered by osteoid was expressed as the ratio of osteoid surface area to bone surface area. All experiments were performed in triplicate.

Intrabone Injections and Bone Tissue Sample Processing

MDA PCa 118b tumors growing subcutaneously in mice were harvested as previously described (26), washed, and resuspended in PBS in preparation for implantation into the mice. Nu/nu male mice (5–6 weeks old, 10 mice per group) were anesthetized with intramuscular injections of ketamine (100 mg/kg) plus acepromazine (2.5 mg/kg). Aliquots of 1×10^6 of 118b cells were diluted in 5 μl of growth medium and then injected into the distal epiphysis of the right femur of each mouse using a 28-gauge Hamilton needle as previously described (26). The contralateral femur was used as an internal control. Twenty mice were randomized to receive intravenous injections of either saline or $VEGF_{121}$/rGel (14 mg/kg) every other day for 9 d. Treatment began 1 week after tumor placement. Treatment was stopped after five cycles, and the mice were then monitored radiographically once a week for tumor bulk and new bone formation, with no further treatment. Mice were euthanized 8 weeks after tumor placement. Femurs bearing MDA PCa 118b tumors and the contralateral non–tumor-bearing femurs were resected, fixed in ethanol, and subjected to micro computed tomography (μCT) analysis to assess bone mass, as previously described (26). MicroCT was performed in the Small Animal Imaging Facility at MD Anderson Cancer Center. The ratio of bone volume to total volume was calculated as previously described (26). Fixed specimens were subsequently decalcified, embedded in paraffin, and sectioned as previously described (29). Histopathologic analysis included H&E, toluidine blue (osteoblasts) and tartrate-resistant acid phosphatase (TRAP) staining (osteoclasts) (26;32). The total tumor content in bone samples was determined as previously described (26). Overall tumor burden was defined as the sum of tumor soft tissue and mineralized tissue.

Statistical Analysis

All statistical analyses were done with Microsoft Excel software (Microsoft, Redmond, WA). Data are presented as means ± SEM. *P* values were obtained using the 2-tailed *t* test with 95% confidence intervals to evaluate statistical significance; $P < 0.05$ was considered statistically significant.

Results

PMOs and the Mouse Preosteoblastic Cell Line MC3T3 Express VEGFR-1, whereas PCa Cells Express Little or No VEGFR

RT-PCR analysis revealed that MC3T3 cells expressed high levels of VEGFR-1 mRNA but did not express the VEGFR-2 transcript (Fig. 1A), suggesting that osteoblasts are candidates for targeting by $VEGF_{121}$/rGel.

We also assessed the expression of VEGFRs in human PCa cells known to induce osteolytic or osteoblastic lesions *in vivo* and found that the osteolytic PC-3 PCa cell line expressed low levels of both VEGFR-1 and VEGFR-2. However, no VEGFR-1 or VEGFR-2 transcripts were detected in two other PCa cell lines, LNCaP and MDA PCa 2b (Fig. 1A). VEGFR was also not detected in mRNA harvested from MDA PCa 118b tumor tissue (Fig. 1B).

VEGFR-1 Transcript Levels Decrease during Osteoblast Differentiation

We previously showed that VEGFR-1 levels decrease in osteoclast precursor cells at onset of differentiation (8). We assessed whether VEGF receptors on osteoblast precursors undergo a similar fate. RT-PCR analysis revealed that MC3T3 cells exhibited a gradual down-regulation of the VEGFR-1 transcript during differentiation (Fig. 1C). RT-PCR analysis also revealed low levels of $VEGF_{164}$ and $VEGF_{120}$ murine isoforms but no $VEGF_{188}$ isoform, suggesting that these precursors promote angiogenesis or mitogenesis in the tumor microenvironment before differentiation.

$VEGF_{121}$/rGel Has Cytotoxic Effects on Osteoblasts but Not on PCa Cells

To determine whether $VEGF_{121}$/rGel could directly target osteoblasts, we evaluated the effect of $VEGF_{121}$/rGel on PMOs and MC3T3 cells grown in differentiation medium for 0–3 weeks. The 50% inhibitory concentration (IC_{50}) of $VEGF_{121}$/rGel on the PMOs was 15 nM, whereas the IC_{50} of rGel alone was 200 nM, indicating that the cytotoxicity of $VEGF_{121}$/rGel was mediated through $VEGF_{121}$ (Fig. 1D). This IC_{50} is similar to that previously reported for mouse osteoclast precursor cells and bone marrow monocytes (8). As expected, we found that MC3T3 sensitivity to $VEGF_{121}$/rGel was significantly reduced when the cells were grown in differentiation medium (Table 1), a finding that matched the PCR data showing down-regulation of VEGFR-1 during differentiation. Confirming the absence of VEGF receptors that bind to $VEGF_{121}$/rGel, we observed no specific cytotoxicity of this construct on the MDA PCa 2b, C4-2B, or MDA PCa 118b PCa cells (Table 1).

$VEGF_{121}$/rGel Internalization into PMOs Is Driven by $VEGF_{121}$

Immunostaining revealed that $VEGF_{121}$/rGel, but not rGel alone, localized in the cytoplasm of PMOs, which suggests that $VEGF_{121}$ mediates rGel internalization (Fig. 1E).

$VEGF_{121}$/rGel Inhibits PCa-Mediated Bone Formation in Neonatal Mouse Calvariae

Organ-culture assays revealed that calvariae treated with medium alone did not show new bone formation, whereas coculturing them with MDA PCa 2b cells stimulated new bone formation (Fig. 2A, upper panel). The addition of 100 nM $VEGF_{121}$/rGel inhibited MDA PCa 2b–cell induced new bone formation (Fig. 2A, lower panel), whereas treatment with $VEGF_{121}$/rGel alone did not have a significant effect on new bone formation (Supplemental Figure 1). Histomorphometric analysis of undecalcified mouse calvariae revealed that $VEGF_{121}$/rGel inhibited PCa-induced new bone formation, as assessed by osteoid-related parameters. The ratio of osteoid volume to bone volume normalized to control decreased by 63% in the presence of $VEGF_{121}$/rGel ($P < 0.05$; double-sided *t* test; Fig. 2B). Similarly, the ratio of osteoid surface to bone surface decreased by 54% (Fig. 2B), and the total osteoid

area decreased by 55% ($P < 0.075$; double-sided *t* test; Fig. 2B). These results suggest that $VEGF_{121}$/rGel can block PCa-induced new bone formation.

$VEGF_{121}$/rGel Inhibits the Osteoblastic Growth of MDA PCa 118b Cells in Bone

Eight weeks after MDA PCa 118b tumor-bearing mice were injected with either saline or $VEGF_{121}$/rGel, 90% (9 of 10) of the saline-treated mice developed robust osteoblastic lesions in their right femurs, an indication of tumor growth (Fig. 3A). In contrast, only 25% (2 of 8) of the $VEGF_{121}$/rGel–treated mice developed areas of osteoblastic reaction in their right femurs. The areas of increased bone density in the treated group were not associated with major alterations in the architecture of the epiphysis (Fig. 3A), indicating a significant reduction of tumor burden in the $VEGF_{121}$/rGel–treated mice. Accordingly, μCT analysis revealed that the total bone volume in the femurs injected with MDA PCa 118b cells was significantly higher in the saline-treated mice than in the $VEGF_{121}$/rGel–treated mice ($P = 0.011$; two-tailed *t* test) (Fig. 3B and C) and that the total bone volume of the femurs injected with MDA PCa 118b cells was essentially the same as the total bone volume of the contralateral femurs in the $VEGF_{121}$/rGel–treated mice (Fig. 3C). MicroCT analysis of a 1-mm cortical segment of each bone's midshaft revealed that the femurs in the $VEGF_{121}$/rGel–treated mice had higher bone mineral density than did those of the saline-treated mice ($P < 0.005$; two-tailed *t* test) (Fig. 3D). We found no significant difference in the overall bone mineral content between the saline- and $VEGF_{121}$/rGel–treated mice ($P < 0.25$; two-tailed *t* test; Fig. 3E), suggesting that the lower bone mineral density in the saline-treated mice was due to the distribution of the bone mineral content over a larger volume.

$VEGF_{121}$/rGel Reduces Osteoblastic PCa Tumor Burden

Histopathologic analysis of the femurs injected with MDA PCa 118b cells in the saline- and $VEGF_{121}$/rGel–treated mice confirmed the presence of osteoblastic lesions in the tumor-bearing legs of all saline-treated mice (Fig. 4A). In contrast, osteoblastic growth of MDA PCa 118b cells was severely impaired in the majority of femurs of the $VEGF_{121}$/rGel–treated mice (Figs. 4B–E). Only isolated pockets of MDA PCa 118b cells were visible in some areas of the right femurs in the $VEGF_{121}$/rGel–treated mice (Fig. 4C). It was notable that no tumor cells were visible in the bone shafts of two $VEGF_{121}$/rGel–treated mice (Figs. 4D and E). None of the mice's contralateral legs showed evidence of osteoblastic lesions (Fig. 4F).

To further understand the effect of $VEGF_{121}$/rGel treatment on tumor growth, we quantified the total tumor burden in bone. The percentage of tumor soft tissue (i.e., tumor cells and stroma) in bone as a function of overall bone volume was significantly reduced in $VEGF_{121}$/rGel–treated mice relative to that in saline-treated mice (mean values, 18.8% vs 33.1%; $P < 0.05$, two-tailed *t* test; overall reduction, 43.2%) (Fig. 4G). Similar results were observed for the overall tumor burden (i.e., tumor soft tissue and new bone matrix), suggesting that reduction in overall tumor burden may be directly correlated to the reduction in tumor cells (mean values, 36.7% vs 52.9%; $P < 0.05$, two-tailed *t* test; overall reduction, 30.6%) (Fig. 4H). Thus, $VEGF_{121}$/rGel statistically significantly prevented tumor growth in bone.

$VEGF_{121}$/rGel Reduces the Number of Osteoclasts at the Tumor–Bone Interface but Not the Number of Peritumoral Osteoblasts

As an indirect measure of the effect of $VEGF_{121}$/rGel treatment on osteoblast proliferation, we assessed osteoblast numbers at the tumor–bone interface and in the peritumoral space on histologic samples stained with toluidine blue. Osteoblasts were easily identified on the bone surface of morphologically normal bone, whether contralateral or $VEGF_{121}$/rGel-treated bones, in which no tumor was visible (Fig. 5A). As previously reported, MDA PCa 118b cells growing in bone demonstrated an increased number of osteoblasts in the tumor-bearing

legs relative to that in the contralateral normal femur (Figs. 5B). Osteoblasts in the vicinity of surviving tumor cells in $VEGF_{121}$/rGel-treated mice were also observed (Fig. 5C). It was interesting that we counted similar numbers of peritumoral osteoblasts in both saline- and $VEGF_{121}$/rGel-treated specimens (Fig. 5D). Because most PCa osteoblastic lesions have an osteolytic component, we investigated the incidence of multinucleated, TRAP-positive osteoclasts. Almost all bone specimens from the saline-treated mice had TRAP-positive osteoclasts prominently lining the tumor–bone interface (Fig. 5E). Both osteoblasts and osteoclasts were identified near tumor cells that were surrounded by bone matrix (Fig. 5F). However, treatment of MDA PCa 118b tumor–bearing mice with $VEGF_{121}$/rGel dramatically reduced the number of osteoclasts lining the tumor–bone interface (Fig. 5G). Fewer osteoclasts were observed near tumor cells surrounded by bone matrix in $VEGF_{121}$/rGel-treated mice, whereas osteoblast numbers were unchanged (Fig. 5G and 5H). Quantification of the overall number of osteoclasts revealed a significant reduction (54%; $P < 0.05$, two-tailed *t* test) in $VEGF_{121}$/rGel–treated specimens relative to that in the saline-treated mice (Fig. 5I).

Discussion

In this study, we obtained evidence that targeting neovascularization, osteoblasts, and osteoclasts effectively controls the osteoblastic progression of PCa cells in bone. Briefly, $VEGF_{121}$/rGel a) specifically targeted osteoblast precursors *in vitro*, b) had no cytotoxic effect against PCa cells *in vitro*, c) inhibited PCa-induced new bone formation in an organ culture assay, d) blocked osteoblastic PCa growth *in vivo*, and e) significantly reduced the number of tumor-associated osteoclasts.

These findings implicate VEGF and its receptors in the progression of PCa metastasis (16;33–36) and suggest that tumor-induced bone remodeling is a central step in skeletal growth. In addition to its angiogenesis-regulating function in bone formation, VEGFR-1 is involved in recruiting osteoclast precursors to the site of bone resorption and osteoclastogenesis (37–39). VEGFR-1 has also been implicated in the maintenance of bone marrow functions in *op/op* mice, with tyrosine kinase–deficient VEGFR-1 and reduced numbers of osteoclasts and osteoblasts (40). Kitagawa et al. (17) reported that mouse osteoblasts express VEGFR-1 and neuropilin-1 and demonstrate activity of PTK787, a tyrosine kinase inhibitor that binds to the ATP binding sites of VEGFRs, against PCa-induced osteoblastic lesions in bone. Otsuka et al. (41) demonstrated that administering bevacizumab to mice bearing experimental bone metastases reduced the tumor-induced formation of osteoblastic lesions. No TRAP-positive osteoclasts were observed in these lesions, even though the osteoblastic bone metastases were smaller in the bevacizumab-treated mice than they were in control mice. These studies' findings suggest that VEGF receptors not targeted by $VEGF_{121}$ are also involved in the development and progression of osteoblastic and osteolytic lesions and are consistent with our finding that VEGF plays a role in this process.

We previously reported that $VEGF_{121}$/rGel readily targets $CD11b^+VEGFR\text{-}1^+$ osteoclast precursor cells, which are derived from bone marrow, *in vitro*. $VEGF_{121}$/rGel may target other $VEGFR\text{-}1^+$ or $VEGFR\text{-}2^+$ cells that may play a role in tumor growth in bone. A subset of VEGFR-expressing, bone marrow–derived cells—primarily $VEGFR\text{-}1^+$ hematopoietic progenitor cells and $VEGFR\text{-}2^+$ circulating endothelial progenitor cells—have been shown to migrate from the bone marrow to metastasis sites in organs, where they create microenvironments conducive to the efficient development of secondary tumors (42). Indeed, Erler et al. (43) have shown that $CD11b^+$ cell recruitment is necessary for the formation of a premetastatic niche and subsequent metastasis of MDA-MB-231 and 4T1/luc breast cancer cells. Other investigators (44;45) have shown that the recruitment of

$CD11b^+VEGFR\text{-}1^+$ cells of various lineages plays a role in the establishment and growth of metastases. Studies to identify other $VEGFR\text{-}1^+/VEGFR\text{-}2^+$ cell populations that may play a role in tumor growth in bone are currently under way in our laboratory.

The process of metastasis involves a sequential series of events, including tumor cell entry into the circulation, arrest in the capillary beds of distant organs, extravasation, and proliferation within the organ parenchyma (46). One caveat of the MDA PCa 118b intrabone-injection system that we used in this study is that it does not recapitulate the entire process of bone metastasis. However, it does adequately recapitulate the process of PCa progression in bone, and thus, the results from our studies are relevant to the effect of $VEGF_{121}$/rGel in established bone metastases of PCa.

We previously reported that $VEGF_{121}$/rGel inhibits angiogenesis (23–25) and reduces the number of osteoclasts at the tumor–bone interface in a PCa model of osteolytic bone growth (8). In this study, we found that $VEGF_{121}$/rGel also targets osteoblast precursors. The reduction in overall tumor burden in $VEGF_{121}$/rGel-treated mice corresponded to a reduction in the overall number of osteoclasts. However, we did not find a reduction in the numbers of peritumoral osteoblasts in treated bone specimens relative to those in controls. These findings suggest that $VEGF_{121}$/rGel affects primarily osteoblast function (including osteoclast activation) rather than osteoblast numbers *in vivo*. These results may also indicate that although targeting osteoblast precursors may affect the initial stages of tumor development, surviving tumor cells retain the ability to recruit osteoblasts effectively on cessation of treatment, which occurred 6 weeks prior to tissue harvest. In summary, our study indicates that the survival advantage of PCa cells was marginalized by the cytotoxic effect of the treatment on osteoblast and osteoclast precursor cells and on the ability of the latter to differentiate to mature osteoclasts.

Two interesting $VEGF_{121}$ fusion toxins have recently been reported in the literature. Smagur et al. (47) recently reported fusing Abrin, a potent plant toxin, to $VEGF_{121}$. Unlike $VEGF_{121}$/rGel, the $VEGF_{121}$ moiety is at the C-terminus. Also unlike $VEGF_{121}$/rGel, the fusion construct did not express as a soluble protein in E. coli and was refolded. The cytotoxicity profile against endothelial cells, which are targeted via VEGFR-2, appears to be similar to that of $VEGF_{121}$/rGel. Because access to receptor-binding determinants can depend on molecular orientation, it will be interesting to see if the construction design of Abrin-$VEGF_{121}$ results in a different activity profile than $VEGF_{121}$/rGel against osteoclast precursor cells, which are effectively targeted via VEGFR-1. A more recent $VEGF_{121}$ fusion construct is SLT-VEGF, a fusion protein comprising $VEGF_{121}$ and catalytically active A subunit of Shiga-like toxin 1 (SLT-1) (48). SLT-VEGF is internalized through VEGFR-2 mediated endocytosis, and its cytotoxicity correlates with VEGFR-2 expression. In addition, this protein exhibits efficacy in a clinically relevant orthotopic nude mouse model of pancreatic cancer. The authors reported that SLT itself can bind to the cellular receptor globotriaosylceramide known as Gb3/CD77 and enter cells through CD77-mediated endocytosis (48). This increases the potential of non-specific toxicity should the fusion protein be cleaved during circulation. In contrast, Gelonin cannot traverse the mammalian cell membrane without a carrier. The authors also reported that modification of SLT-VEGF with no more than one molecule of Cy5 dye resulted in a greater than 50-fold reduction in the IC_{50}, which may be the result of modification of VEGF lysine residues that are critically involved in the interaction of VEGF with VEGFR-2. In contrast, IC_{50} of $VEGF_{121}$/rGel labeled with ^{64}Cu-DOTA (average of 3.3 DOTAmolecules per $VEGF_{121}$/rGel molecule) did not significantly change compared to $VEGF_{121}$/rGel alone, allowing multimodality imaging of tumor growth (49).

Our results indicate that $VEGF_{121}$/rGel has a significant therapeutic effect against the osteoblastic progression of metastatic PCa cells and that the antitumor effect is mediated by targeting PCa stroma. Because PCa development in bone appears to be dependent on tumor-induced bone remodeling, trials of agents targeting multiple bone-cell components, such as $VEGF_{121}$/rGel alone or in combination with conventional chemotherapeutic agents, may enable a better understanding of the relative effect of each of the processes involved in new bone formation and metastasis, such as tumor homing, recruitment of osteoclast and osteoblast precursors, and the role of the stroma. $VEGF_{121}$/rGel treatment is a novel concept of a single agent targeting several bone-cell components and may form the basis for combination therapies with cytotoxic agents for skeletal tumors in their most lethal phase.

Supplementary Material

Refer to Web version on PubMed Central for supplementary material.

Acknowledgments

Financial Support: This research was conducted in part by the Clayton Foundation for Research (M.G.R.) and was supported by a grant from the National Institutes of Health, R01 CA96797 (to N.M.N.), and in part by the National Institutes of Health through MD Anderson Cancer Center's Support Grant CA016672.

We acknowledge the support of the Rolanette and Berdon Laurence Bone Disease Program of Texas to our Bone Histomorphometry Core. We appreciate the assistance of Karen F. Phillips, ELS, and Joseph A. Munch in editing this manuscript.

References

1. Vessella RL, Corey E. Targeting factors involved in bone remodeling as treatment strategies in prostate cancer bone metastasis. Clin Cancer Res. 2006; 12:6285s–90s. [PubMed: 17062715]
2. Jemal A, Siegel R, Ward E, et al. Cancer statistics, 2009. CA Cancer J Clin. 2009; 59:225–49. [PubMed: 19474385]
3. Lange PH, Vessella RL. Mechanisms, hypotheses and questions regarding prostate cancer micrometastases to bone. Cancer Metastasis Rev. 1998; 17:331–6. [PubMed: 10453276]
4. Galasko CS. Mechanisms of lytic and blastic metastatic disease of bone. Clin Orthop Relat Res. 1982:20–7. [PubMed: 7105580]
5. Goltzman D. Mechanisms of the development of osteoblastic metastases. Cancer. 1997; 80:1581–7. [PubMed: 9362425]
6. Koeneman KS, Yeung F, Chung LW. Osteomimetic properties of prostate cancer cells: a hypothesis supporting the predilection of prostate cancer metastasis and growth in the bone environment. Prostate. 1999; 39:246–61. [PubMed: 10344214]
7. Koutsilieris M. Osteoblastic metastasis in advanced prostate cancer. Anticancer Res. 1993; 13:443–9. [PubMed: 8517661]
8. Mohamedali KA, Poblenz AT, Sikes CR, et al. Inhibition of prostate tumor growth and bone remodeling by the vascular targeting agent VEGF121/rGel. Cancer Res. 2006; 66:10919–28. [PubMed: 17108129]
9. Lee RJ, Saylor PJ, Smith MR. Treatment and prevention of bone complications from prostate cancer. Bone. 2010
10. Carlevaro MF, Cermelli S, Cancedda R, Descalzi CF. Vascular endothelial growth factor (VEGF) in cartilage neovascularization and chondrocyte differentiation: auto-paracrine role during endochondral bone formation. J Cell Sci. 2000; 113 (Pt 1):59–69. [PubMed: 10591625]
11. Horner A, Bishop NJ, Bord S, et al. Immunolocalisation of vascular endothelial growth factor (VEGF) in human neonatal growth plate cartilage. J Anat. 1999; 194 (Pt 4):519–24. [PubMed: 10445820]

12. Street J, Bao M, deGuzman L, et al. Vascular endothelial growth factor stimulates bone repair by promoting angiogenesis and bone turnover. Proc Natl Acad Sci U S A. 2002; 99:9656–61. [PubMed: 12118119]
13. Zelzer E, McLean W, Ng YS, et al. Skeletal defects in VEGF(120/120) mice reveal multiple roles for VEGF in skeletogenesis. Development. 2002; 129:1893–904. [PubMed: 11934855]
14. Zelzer E, Mamluk R, Ferrara N, et al. VEGFA is necessary for chondrocyte survival during bone development. Development. 2004; 131:2161–71. [PubMed: 15073147]
15. Mayr-Wohlfart U, Waltenberger J, Hausser H, et al. Vascular endothelial growth factor stimulates chemotactic migration of primary human osteoblasts. Bone. 2002; 30:472–7. [PubMed: 11882460]
16. Dai J, Kitagawa Y, Zhang J, et al. Vascular endothelial growth factor contributes to the prostate cancer-induced osteoblast differentiation mediated by bone morphogenetic protein. Cancer Res. 2004; 64:994–9. [PubMed: 14871830]
17. Kitagawa Y, Dai J, Zhang J, et al. Vascular endothelial growth factor contributes to prostate cancer-mediated osteoblastic activity. Cancer Res. 2005; 65:10921–9. [PubMed: 16322239]
18. Blanchard F, Duplomb L, Baud'huin M, Brounais B. The dual role of IL-6-type cytokines on bone remodeling and bone tumors. Cytokine Growth Factor Rev. 2009; 20:19–28. [PubMed: 19038573]
19. Casimiro S, Guise TA, Chirgwin J. The critical role of the bone microenvironment in cancer metastases. Mol Cell Endocrinol. 2009; 310:71–81. [PubMed: 19616059]
20. McMahon G. VEGF receptor signaling in tumor angiogenesis. Oncologist. 2000; 5 (Suppl 1):3–10. [PubMed: 10804084]
21. Gille H, Kowalski J, Li B, et al. Analysis of biological effects and signaling properties of Flt-1 (VEGFR-1) and KDR (VEGFR-2). A reassessment using novel receptor-specific vascular endothelial growth factor mutants. J Biol Chem. 2001; 276:3222–30. [PubMed: 11058584]
22. Shibuya M. Role of VEGF-flt receptor system in normal and tumor angiogenesis. Adv Cancer Res. 1995; 67:281–316. [PubMed: 8571818]
23. Mohamedali KA, Kedar D, Sweeney P, et al. The vascular-targeting fusion toxin VEGF121/rGel inhibits the growth of orthotopic human bladder carcinoma tumors. Neoplasia. 2005; 7:912–20. [PubMed: 16242074]
24. Ran S, Mohamedali KA, Luster TA, Thorpe PE, Rosenblum MG. The vascular-ablative agent VEGF(121)/rGel inhibits pulmonary metastases of MDA-MB-231 breast tumors. Neoplasia. 2005; 7:486–96. [PubMed: 15967101]
25. Veenendaal LM, Jin H, Ran S, et al. In vitro and in vivo studies of a VEGF121/rGelonin chimeric fusion toxin targeting the neovasculature of solid tumors. Proc Natl Acad Sci U S A. 2002; 99:7866–71. [PubMed: 12060733]
26. Li ZG, Mathew P, Yang J, et al. Androgen receptor-negative human prostate cancer cells induce osteogenesis in mice through FGF9-mediated mechanisms. J Clin Invest. 2008; 118:2697–710. [PubMed: 18618013]
27. Kroll J, Waltenberger J. A novel function of VEGF receptor-2 (KDR): rapid release of nitric oxide in response to VEGF-A stimulation in endothelial cells. Biochem Biophys Res Commun. 1999; 265:636–9. [PubMed: 10600473]
28. Waltenberger J, Claesson-Welsh L, Siegbahn A, Shibuya M, Heldin CH. Different signal transduction properties of KDR and Flt1, two receptors for vascular endothelial growth factor. J Biol Chem. 1994; 269:26988–95. [PubMed: 7929439]
29. Yang J, Fizazi K, Peleg S, et al. Prostate cancer cells induce osteoblast differentiation through a Cbfa1-dependent pathway. Cancer Res. 2001; 61:5652–9. [PubMed: 11454720]
30. Yamauchi M, Yamaguchi T, Kaji H, Sugimoto T, Chihara K. Involvement of calcium-sensing receptor in osteoblastic differentiation of mouse MC3T3-E1 cells. Am J Physiol Endocrinol Metab. 2005; 288:E608–E616. [PubMed: 15547142]
31. Navone NM, Olive M, Ozen M, et al. Establishment of two human prostate cancer cell lines derived from a single bone metastasis. Clin Cancer Res. 1997; 3:2493–500. [PubMed: 9815652]
32. Lee YP, Schwarz EM, Davies M, et al. Use of zoledronate to treat osteoblastic versus osteolytic lesions in a severe-combined-immunodeficient mouse model. Cancer Res. 2002; 62:5564–70. [PubMed: 12359769]

33. Chen J, De S, Brainard J, Byzova TV. Metastatic properties of prostate cancer cells are controlled by VEGF. Cell Commun Adhes. 2004; 11:1–11. [PubMed: 15500293]
34. Ismail AH, Altaweel W, Chevalier S, Kassouf W, Aprikian AG. Expression of vascular endothelial growth factor-A in human lymph node metastases of prostate cancer. Can J Urol. 2004; 11:2146–50. [PubMed: 15003156]
35. Shariat SF, Anwuri VA, Lamb DJ, et al. Association of preoperative plasma levels of vascular endothelial growth factor and soluble vascular cell adhesion molecule-1 with lymph node status and biochemical progression after radical prostatectomy. J Clin Oncol. 2004; 22:1655–63. [PubMed: 15117988]
36. Zeng Y, Opeskin K, Baldwin ME, et al. Expression of vascular endothelial growth factor receptor-3 by lymphatic endothelial cells is associated with lymph node metastasis in prostate cancer. Clin Cancer Res. 2004; 10:5137–44. [PubMed: 15297417]
37. Gerber HP, Vu TH, Ryan AM, et al. VEGF couples hypertrophic cartilage remodeling, ossification and angiogenesis during endochondral bone formation. Nat Med. 1999; 5:623–8. [PubMed: 10371499]
38. Matsumoto Y, Tanaka K, Hirata G, et al. Possible involvement of the vascular endothelial growth factor-Flt-1-focal adhesion kinase pathway in chemotaxis and the cell proliferation of osteoclast precursor cells in arthritic joints. J Immunol. 2002; 168:5824–31. [PubMed: 12023386]
39. Niida S, Kaku M, Amano H, et al. Vascular endothelial growth factor can substitute for macrophage colony-stimulating factor in the support of osteoclastic bone resorption. J Exp Med. 1999; 190:293–8. [PubMed: 10432291]
40. Niida S, Kondo T, Hiratsuka S, et al. VEGF receptor 1 signaling is essential for osteoclast development and bone marrow formation in colony-stimulating factor 1-deficient mice. Proc Natl Acad Sci U S A. 2005; 102:14016–21. [PubMed: 16172397]
41. Otsuka S, Hanibuchi M, Ikuta K, et al. A bone metastasis model with osteolytic and osteoblastic properties of human lung cancer ACC-LC-319/bone2 in natural killer cell-depleted severe combined immunodeficient mice. Oncol Res. 2009; 17:581–91. [PubMed: 19806789]
42. Kaplan RN, Riba RD, Zacharoulis S, et al. VEGFR1-positive haematopoietic bone marrow progenitors initiate the pre-metastatic niche. Nature. 2005; 438:820–7. [PubMed: 16341007]
43. Erler JT, Bennewith KL, Cox TR, et al. Hypoxia-induced lysyl oxidase is a critical mediator of bone marrow cell recruitment to form the premetastatic niche. Cancer Cell. 2009; 15:35–44. [PubMed: 19111879]
44. Qian B, Deng Y, Im JH, et al. A distinct macrophage population mediates metastatic breast cancer cell extravasation, establishment and growth. PLoS One. 2009; 4:e6562. [PubMed: 19668347]
45. Yang L, Huang J, Ren X, et al. Abrogation of TGF beta signaling in mammary carcinomas recruits Gr-1+CD11b+ myeloid cells that promote metastasis. Cancer Cell. 2008; 13:23–35. [PubMed: 18167337]
46. Langley RR, Fidler IJ. Tumor cell-organ microenvironment interactions in the pathogenesis of cancer metastasis. Endocr Rev. 2007; 28:297–321. [PubMed: 17409287]
47. Smagur A, Boyko MM, Bironi NV, Cichon T, Szala S. Chimeric protein ABRaA-VEGF121 is cytotoxic towards VEGFR-2-expressing PAE cells and inhibits B16-F10 melanoma growth. Acta Biochim Pol. 2009; 56:115–24. [PubMed: 19252752]
48. Hotz B, Backer MV, Backer JM, Buhr HJ, Hotz HG. Specific targeting of tumor endothelial cells by a shiga-like toxin-vascular endothelial growth factor fusion protein as a novel treatment strategy for pancreatic cancer. Neoplasia. 2010; 12:797–806. [PubMed: 20927318]
49. Hsu AR, Cai W, Veeravagu A, et al. Multimodality molecular imaging of glioblastoma growth inhibition with vasculature-targeting fusion toxin VEGF121/rGel. J Nucl Med. 2007; 48:445–54. [PubMed: 17332623]

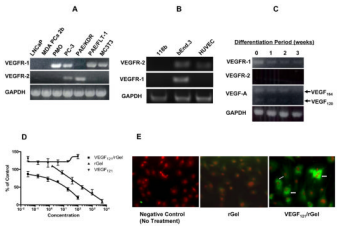

Figure 1.

(A–C) RT-PCR analysis. VEGFR primers that recognize conserved sequences in both mouse and human cDNA that result in an identical length of transcript were used. *(A)* LNCaP and MDA PCa 2b human prostate cancer cells showed no PCR product for VEGFR-1 or VEGFR-2. PC-3 cells expressed low levels of transcript for both VEGFR-1 and VEGFR-2. Primary mouse osteoblasts (PMOs) and MC3T3 cells expressed VEGFR-1 but not VEGFR-2. mRNA transcript from cells expressing human VEGFR-1 (PAE/FLT-1) and VEGFR-2 (PAE/KDR) were used as controls. (*B*) MDA PCa 118b tumor tissue did not express VEGFR-1 or VEGFR-2. Murine bEnd.3 cells and human umbilical vein endothelial cells (HUVECs) were used as controls. GAPDH was utilized as a loading control. (*C*) VEGFR-1 mRNA was down-regulated during MC3T3 cell differentiation. VEGFR-1, VEGFR-2, and VEGF-A levels are shown. GAPDH primers were used as controls. Low levels of $VEGF_{164}$ and $VEGF_{120}$ transcripts were also detected. *(D–E)* $VEGF_{121}$/rGel is specifically targeted to primary mouse osteoblasts (PMOs). (*D*) $VEGF_{121}$/rGel, rGel, and $VEGF_{121}$ cytotoxicity on PMOs over 72 h. Each experiment was performed in triplicate. (*E*) $VEGF_{121}$/rGel internalization into PMOs was driven by $VEGF_{121}$. PMOs were treated with either 10 nM $VEGF_{121}$/rGel or the untargeted toxin rGel for 24 h. Only nuclei were visible in rGel-treated PMOs whereas fluorescent rGel staining was observed in the cytoplasm of $VEGF_{121}$/rGel-treated PMOs (arrows).

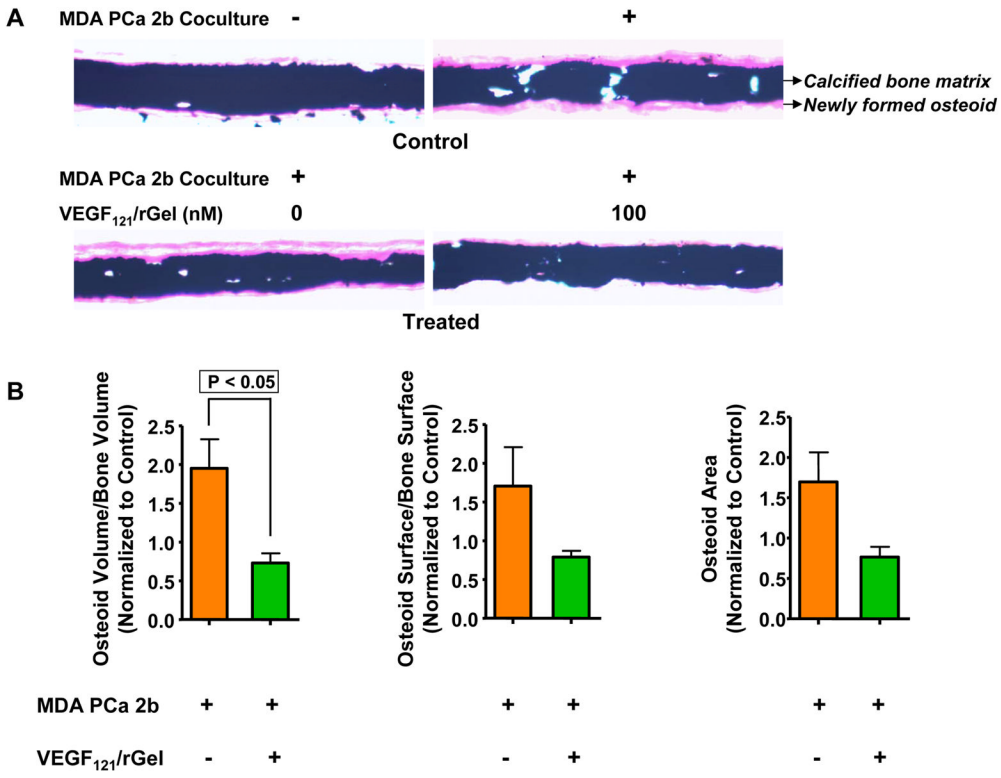

Figure 2.

(*A*) $VEGF_{121}$/rGel inhibited prostate cancer–induced bone formation. Upper panel: representative neonatal mouse calvariae cultured *in vitro* in the absence (left) or presence (right) of MDA PCa 2b cells. Lower panel: representative neonatal mouse calvariae cocultured with MDA PCa 2b cells in the absence (left) and presence (right) of 100 nM $VEGF_{121}$/rGel. Calcified bone matrix and newly formed osteoid are indicated. (*B*) Quantification of $VEGF_{121}$/rGel's effect on new bone formation. $VEGF_{121}$/rGel significantly decreased the ratio of osteoid volume to bone volume (left panel) primarily by reducing osteoid surface (middle panel) and area (right panel).

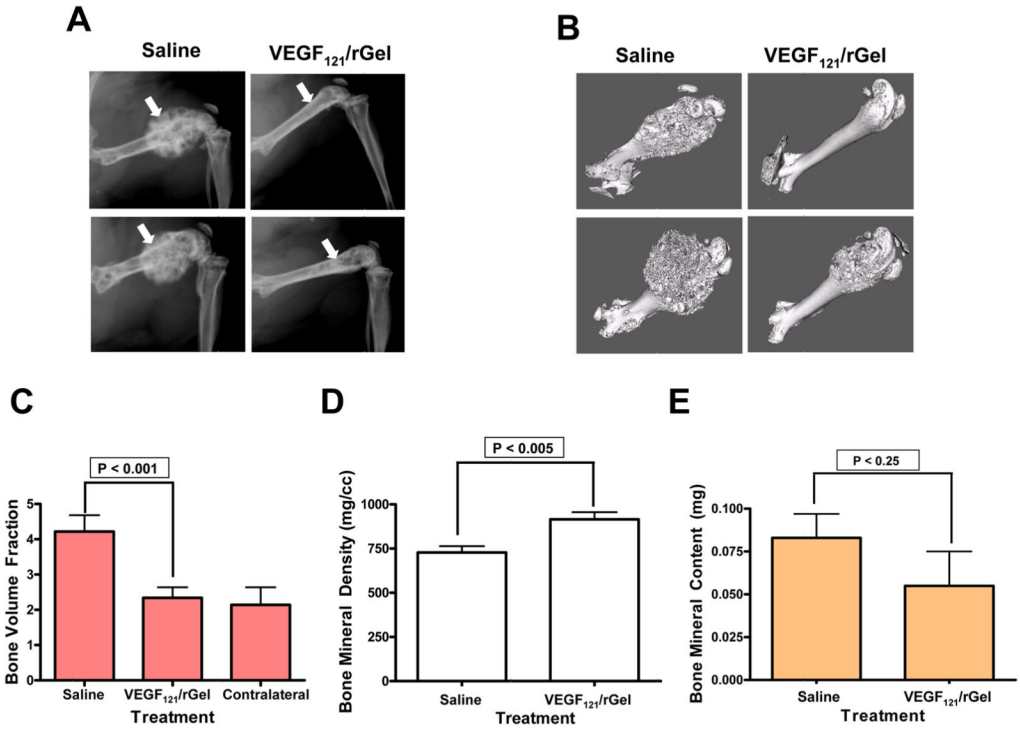

Figure 3.

$VEGF_{121}$/rGel inhibited osteoblastic growth of MDA PCa 118b cells in bone. (*A*) Radiographic analysis of saline- and $VEGF_{121}$/rGel–treated mice. Radiographs show right femurs 8 weeks after implantation of MDA PCa 118b cells. Arrows indicate the increased bone density in the saline-treated mice (left panels) and significantly lower bone density in the $VEGF_{121}$/rGel–treated mice (right panels). (*B*) Representative microcomputed tomography (μCT) images reveal higher bone mass in the tumor-bearing femurs of saline-treated mice (left panels) than in the tumor-bearing femurs of $VEGF_{121}$/rGel–treated mice (right panels). (*C*) Quantification of μCT data revealed that $VEGF_{121}$/rGel normalized the bone volume fraction of 118b tumor-containing bone, as compared with the contralateral bone in the $VEGF_{121}$/rGel-treated mice. (*D*) $VEGF_{121}$/rGel treatment increased bone mineral density and reduced overall bone volume. (*E*) However, $VEGF_{121}$/rGel treatment did not significantly affect overall bone mineral content.

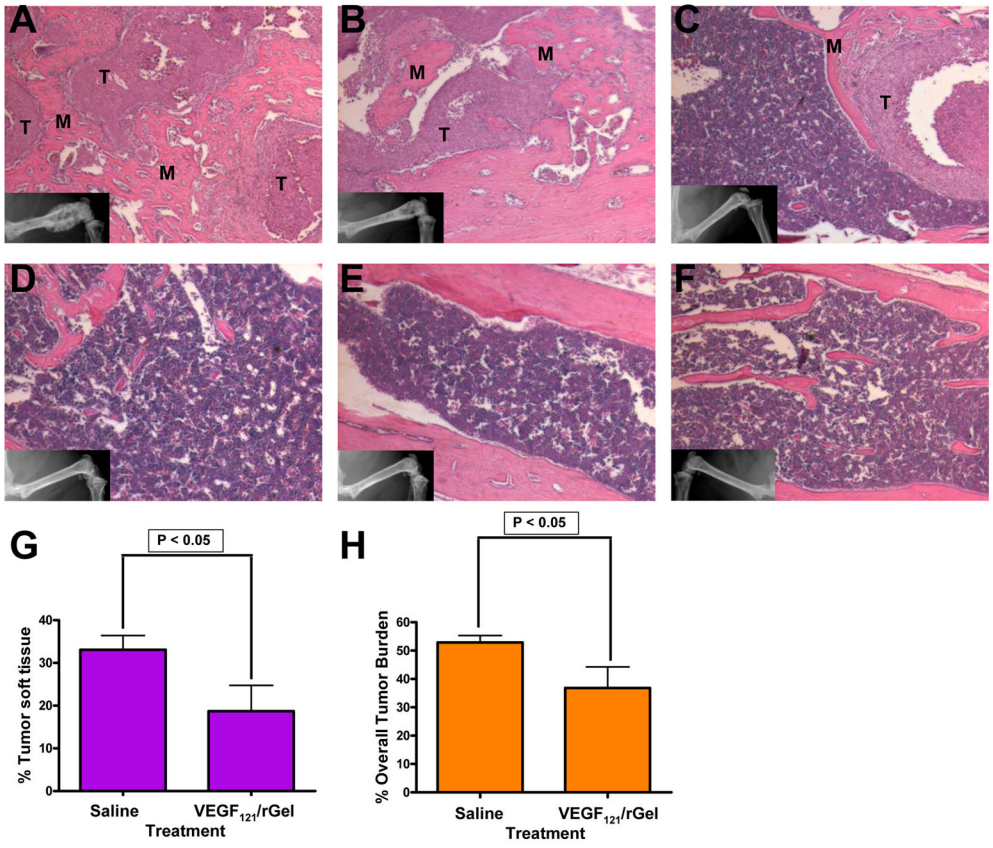

Figure 4.

$VEGF_{121}$/rGel inhibited osteoblastic growth of MDA PCa 118b cells in bone. (*A–F*) H&E staining of MDA PCa 118b tumors in the femurs of nude mice. T, prostate cancer cells; M, bone matrix. Insets represent Faxitron images of bone specimens at the time of harvest. (*A*) Representative femur from a 118b tumor–bearing leg of a saline-treated mouse. (*B–E*) Tumor-bearing femurs from $VEGF_{121}$/rGel–treated mice with varying levels of tumor growth. (*B*) Visible, but reduced, osteoblastic growth of tumor cells. (*C*) Isolated pocket of tumor cells in the diaphyseal region of a femur, exhibiting limited osteoblastic growth. (*D, E*) Tumor-free femurs from two $VEGF_{121}$/rGel–treated mice. (*F*) Contralateral leg. No tumors were observed in the contralateral legs of any mice in the study. (*G*) Quantitative analysis of tumor soft tissue as a percentage of total bone volume showed a significant reduction of prostate cancer cells in the femurs of $VEGF_{121}$/rGel–treated mice relative to those in the saline-treated mice. (*H*) Overall tumor burden (tumor soft tissue + new bone matrix) was also significantly reduced in $VEGF_{121}$/rGel–treated mice relative to that in saline-treated mice.

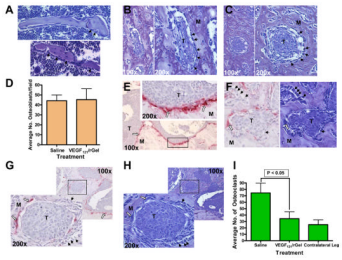

Figure 5.

VEGF$_{121}$/rGel reduced the number of osteoclasts at the tumor–bone interface but did not reduce peritumoral osteoblasts. T, prostate cancer cells; M, bone matrix; black arrows, osteoblasts; white arrows, osteoclasts. (*A*) Toluidine blue staining of contralateral (top) and tumor-bearing (bottom) femurs shows morphologically normal bone tissue with visible osteoblasts. Original magnification, ×200. (*B*, *C*) Toluidine blue staining of tumor cells that are surrounded by bone matrix: (*B*) control, (*C*) VEGF$_{121}$/rGel. (*D*) Quantitation of peritumoral osteoblasts per field. (*E*) TRAP-positive osteoclasts are present throughout the tumor–bone interface in control mice. Original magnification, ×100; inset original magnification, ×200. (*F*) TRAP (left) and toluidine blue (right) staining of identical specimens from control mice indicate the presence of both osteoclasts and osteoblasts in the vicinity of tumor cells that are surrounded by bone matrix. Original magnification, ×200. (*G*) TRAP and (*H*) toluidine blue staining of identical specimens from VEGF$_{121}$/rGel-treated mice. Fewer osteoclasts line the tumor–bone interface or are present in the vicinity of tumor cells surrounded by bone matrix, while osteoblast numbers are unchanged. Original magnification, ×100. (*I*) Quantification of osteoclasts at the tumor–bone interface revealed that VEGF$_{121}$/rGel significantly suppressed osteoclast numbers compared to controls. Osteoclast numbers in the contralateral leg are provided as a reference.

Table 1

$VEGF_{121}$/rGel and rGel cytotoxicity on MC3T3 cells and prostate cancer cell lines

Cell Line	Cell Type	Status	IC_{50} (nM), $VEGF_{121}$/rGel	IC_{50} (nM), rGel
MC3T3	Mouse preosteoblast	Log phase	30	100
MC3T3	Mouse preosteoblast	Differentiated, 1 week	500	500
MC3T3	Mouse preosteoblast	Differentiated, 2 weeks	> 1000	> 1000
MC3T3	Mouse preosteoblast	Differentiated, 3 weeks	> 1000	> 1000
MDA PCa 2b	Human Prostate	Log phase	290	1150
C4-2B	Human Prostate	Log phase	> 1000	> 1000
MDA PCa 118b	Human Prostate	Log phase	> 1000	> 1000
PC-3	Human Prostate	Log phase	225*	100*

*Veenendaal et al.(25)